Applied Catalysis B: Environmental 209 (2017) 155–160

Contents lists available at ScienceDirect

Applied Catalysis B: Environmental

journal homepage: www.elsevier.com/locate/apcatb

Sulfurated [NiFe]-based layered double hydroxides nanoparticles as efficient co-catalysts for photocatalytic hydrogen evolution using CdTe/CdS quantum dots

Dongting Yue, Xufang Qian, Miao Kan, Meng Ren, Yao Zhu, Lele Jiang, Yixin Zhao *

School of Environmental Science and Engineering, Shanghai Jiao Tong University,800 Dongchuan Rd., Shanghai 200240, China

ARTICLE INFO

Article history:
Received 16 January 2017
Received in revised form 26 February 2017
Accepted 27 February 2017
Available online 1 March 2017

Keywords:
Sulfurated [NiFe]-LDH nanoparticles
[NiFe]-LDH
CdTe/CdS quantum dots
Photocatalytic hydrogen evolution

ABSTRACT

Binary transition metals layered double hydroxides (LDH) such as [NiFe] have been developed as the promising low cost and high performance electrocatalysts for hydrogen evolution. However their applications as co-catalysts in photocatalysis like CdTe/CdS quantum dots (QDs) for hydrogen evolution are limited by their ineffective contact with QDs nanoparticles. We report on the synthesis of the sulfurated [NiFe]-LDH (FeNiS) nanoparticles via the sulfurizing treatment of [NiFe]-based LDH. The sulfurizing treatment can successfully break the 2D [NiFe]-LDH into FeNiS nanoparticles by replacing the OH group via the S group. FeNiS nanoparticles provide more bonding sites for CdTe/CdS QDs due to the sulfur species formed on the FeNiS nanoparticles. The junction between sulfur species and Cd^{2+} of CdTe/CdS QDs could facilitate electrons transfer between CdTe/CdS QDs and FeNiS nanoparticles and then significantly enhance their photocatalytic hydrogen production. The photocatalytic activity of FeNiS-CdTe/CdS is much better than [NiFe]-CdTe/CdS QDs and Pt-CdTe/CdS QDs. In all, this novel FeNiS nanoparticles would be a promising low cost co-catalyst for energy and environmental photocatalysis.

1. Introduction

Photocatalysis is one of most promising technique candidate for environmental remediation and renewable energy for global energy crisis, climate change and environmental pollutant [1–5]. Among photocatalytic renewable energy, hydrogen (H_2) is considered to be an ideal alternative due to its high energy density and a benign combustion product [6–8], particularly as it can be produced by photocatalytic water splitting with solar irritation [9,10]. To more efficient utilization of visible light, using semiconductor quantum dots (QDs) as photosensitizers for light-driven H_2 production has attracted widespread attention due to their unique nanometer-sized physical properties including the quantum confinement effect, broad and intense absorption spectra in the visible light region and special surface properties [11–17]. Up to date, noble elements especially Pt-group metals are dominating catalysts for H_2 evolution reaction [18–23], but their high cost, elemental scarcity and low sulfur tolerance greatly hinder their large scale applications [24–27]. Hence, tremendous efforts are devoted to develop noble-metal-free catalysts with high catalytic activity, stability, and sulfur tolerance. Recently, layered double hydroxides (LDHs), as for 2D nanostructures, have emerged as an interesting family of low-cost materials with high catalytic performance towards both hydrogen evolution reaction (HER) and oxygen reduction reaction (ORR) [28–33]. Latest report demonstrates that [NiFe]-based LDH can even outperform most of the known transition metal catalysts for H_2 evolution in electrolysis [25,34,35]. Surprisingly, despite extensive use of [NiFe]-based LDH as electrode materials for HER and ORR, these [NiFe]-based LDH has been rarely utilized as co-catalysts for photocatalytic H_2 evolution using QDs. The main challenge could be that the 2D structure of hydroxides provides the limited bonding sites for loading QDs, which suppress the photogenerated electron transport from QDs to active sites of [NiFe]-based LDH. Furthermore, the poor electron transfer of hydroxides also accounts for the low catalytic efficiency [31]. To overcome these problems, we constructed the sulfurated [NiFe]-LDH (FeNiS) nanoparticles with more bonding sites and active sites as to co-catalyze the CdTe/CdS QDs with enhanced the photocatalytic performance of H_2 evolution.

In this report, we synthesized FeNiS nanoparticles by the strategy illustrated in Fig. S1. Firstly, we synthesized the [NiFe]-LDH as the precursors via one step hydrothermal method. Then [NiFe]-LDH nanosheets were changed into porous layered structure by sulfurizing treatment. With the continue sulfidation process, the

* Corresponding author.
E-mail address: yixin.zhao@sjtu.edu.cn (Y. Zhao).

http://dx.doi.org/10.1016/j.apcatb.2017.02.075
0926-3373/

formation of FeNiS nanoparticles were induced the destruction of the porous nanosheets, which could lead to improve chemical catalytic performance [36–38]. We combine these FeNiS nanoparticles with CdTe/CdS QDs to form an efficient photocatalyts for H_2 evolution. The CdTe/CdS QDs could be easily bound to the surface of FeNiS nanoparticles due to the presence of more sulfur species. The sulfur species from FeNiS nanoparticles and Cd^{2+} on the surface of CdTe/CdS QDs could connect together, which could promote the intimate combination of FeNiS and CdTe/CdS QDs. Consequently, the H_2 evolution of FeNiS-CdTe/CdS QDs system increases ~32-fold compared with the same system in the absence of FeNiS. In all, FeNiS nanoparticles clearly offer a promising co-catalyst candidate for highly efficient and sulfur tolerant photocatalysts for energy and environmental applications in future.

2. Experimental

2.1. Chemicals

Ferrous nitrate ($Fe(NO_3)_3{\cdot}9H_2O$, 0.02 M), nickel chloride ($NiCl_2{\cdot}6H_2O$, 0.2 M), urea, trisodium citrate (TSC), thioacetamide (TAA), tellurium powder (99.9%), ascorbic acid (H_2A), sodium hydroxide, hydrochloric acid, and ethanol were purchased from Sinopharm Chemical Reagent Co., Ltd. Cadmium chloride ($CdCl_2$), 3-Mercaptopropionic acid (3-MPA), sodium borohydride ($NaBH_4$) (98%), potassium hexachloroplatinate (K_2PtCl_6) were obtained from Aladdin Industrial Corporation. L-glutathione reduced (GSH) (Sigma-Aldrich, ≥ 98.0%) was obtained from InnoChem Science&Technology Co., Ltd.

2.2. Synthesis of CdTe/CdS QDs

The CdTe/CdS QDs were synthesized according to the methods reported in the literature [27]. The experimental details of synthetic method to CdTe/CdS QDs were shown in the Supporting Information.

2.3. Synthesis of sulfurated [NiFe]-LDH nanoparticles

The synthetic route to FeNiS nanoparticles was shown in Fig. S1. The synthetic methods were reported in the literature [25]. In the first step, [NiFe]-LDH were synthesized via the hydrothermal method. Briefly, ferrous nitrate ($Fe(NO_3)_3{\cdot}9H_2O$, 0.02 M), nickel chloride ($NiCl_2{\cdot}6H_2O$, 0.2 M) were dissolved in 70 ml DI water. Then 5.6 ml urea aqueous solution (0.5 M) and 2 ml TSC (0.01 M) were mixed into the above solution with magnetic stirring for 30 min. The solution was then transferred to a 150 ml Teflon lined stainless steel autoclave and heated at 150 °C for 24 h. After centrifugation, washed with water for three times and dried under vacuum condition, [NiFe]-LDH precursor was obtained. The second step of sulfidation was performed, where 100 mg [NiFe]-LDH precursor was dispersed into 40 ml solvent of ethanol, followed by the addition of TAA (1.5 mmol) under the stirring condition of 600 rpm for 2 h. Thereafter, the above solution was transferred into the 150 ml Teflon-lined stainless steel autoclave for hydrothermal reaction at 120 °C for 8 h. The FeNiS nanoparticles were prepared by centrifugated, washed with ethanol three times, and then dried under vacuum condition.

2.4. Procedure for the fabrication of FeNiS-CdTe/CdS QDs photocatalyst

The CdTe/CdS QDs solution and co-catalysts (FeNiS, FeNi) were placed in a sealed gas circulation. The total volume of the aqueous solution was 20 ml. Prior to irradiation, the pH value of the solution was adjusted to 4.5 using an aqueous 1.0 M NaOH or 1.0 M HCl solution. The suspension of the CdTe/CdS QDs tended to form precipitates owing to the protonation of CdTe/CdS QDs surface under acidic conditions. Hence, the H_2 evolution experiment was performed under rapidly rigorous stirring to maintain the CdTe/CdS QDs in suspension. After stirring 30 min, we collected the CdTe/CdS QDs precipitates from the solution using centrifugation, and then dried under vacuum condition. The samples were prepared for further characterization.

2.5. Photocatalytic performance for H_2 generation

The compounds combined with CdTe/CdS QDs and co-catalysts (FeNiS, FeNi, Pt) were placed in a sealed gas circulation with an evacuation system and magnetic stirring. The total volume of the aqueous solution was 20 ml. Prior to irradiation, the pH of the solution was adjusted by 1.0 M NaOH or 1.0 M HCl solution. The solution was then degassed for 20 min to become vacuum. The H_2 evolution experiment was conducted under the irradiation by a 300 W Xe lamp (Ceaulight, CEL-HXF-300) fitted with a 420 nm cutoff filter and maintained at 4 °C by a flow of cooling water during the photocatalysis process. The generated photoproduct of H_2 was characterized by the online gas chromatography (Ceaulight, GC 7900, MS–5 A column, TCD, N_2 carrier). The desired concentration of the reaction system was achieved by adjusting pH and dissolving different amount of H_2A, CdTe/CdS QDs and co-catalysts into 20 ml of the mixed aqueous solution. In addition, after 10 h of irradiation, we collected the precipitates from the solution using centrifugation, and then dried under vacuum condition. The samples were prepared for further analysis.

2.6. Characterization

Powder X-ray diffraction (XRD) patterns were performed on a Shimadzu XRD-6100 diffractometer with Cu-Kα radiation. The data were recorded at a scan rate of 10 deg·min^{-1} in the 2θ range from 5° to 80°. Field-emission scanning electron microscopy (FESEM) measurements were conducted on a JSM-7800F Primescanning electron microscope. The morphologies of samples were characterized by transmission electron microscopy (TEM) and high-resolution transmission electron microscopy (HRTEM) which were performed on a JEM-2100F microscope. X-ray photoelectron spectroscopy (XPS) analysis (PerkinElmer PHI 5000C, AlKa) was carried out to analyze the Surface electronic states of catalysts. All binding energies were calibrated by using the contaminant carbon (C 1s = 284.6 eV) as a reference. The composition of samples was determined by inductively coupled plasma optical emission spectrometer (ICP-AES, iCAP6300, Thermo). The N_2 sorption measurement was performed using Nova-2200 e, and the specific surface area and pore size distribution were calculated using the Brunauer–Emmett–Teller (BET) and Barrett–Joyner–Halenda (BJH) methods, respectively. Photoluminescence (PL) spectra were recorded on a F-380 fluorescence spectrophotometer at room temperature (F-380, Tianjin Gangdong SCI.&TECH. Development CO, LTD). The excitation wavelength for all steady-state PL measurements was set to 410 nm.

3. Results and discussion

The XRD patterns of [NiFe]-LDH and NiFeS samples are shown in Fig. 1. [NiFe]-LDH samples present similar diffraction peaks of (003), (006), (012), (018), and (113) planes of α-$Ni(OH)_2$ but with some shifted, which could be ascribed to the Fe/Ni substitution. This is consistent with previous reports of [NiFe]-LDH [39–41]. Besides the similarity to α-$Ni(OH)_2$, the [NiFe]-LDH samples also exhibit the characteristic diffraction peaks 19.258°, 33.064°, 38.541°, and 52.100°, which can be ascribed to standard (001), (102), (110) and

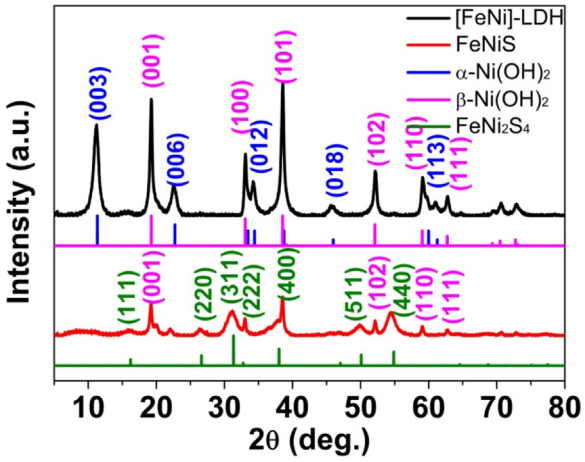

Fig. 1. XRD patterns of [NiFe]-LDH nanosheets and NiFeS nanoparticles. The lines correspond to standard XRD patterns of α-$Ni(OH)_2$ (blue, JCPDS card No. 38-0715), β-$Ni(OH)_2$ (magenta, JCPDS card No. 14-0117), and $FeNi_2S_4$ (green, JCPDS card No. 14-0117). (For interpretation of the references to colour in this figure legend, the reader is referred to the web version of this article.)

(111) planes of β-$Ni(OH)_2$. These results reveal that Ni^{2+} in the α-$Ni(OH)_2$ lattice seems to be more easily replaced by Fe^{3+} than in the β-$Ni(OH)_2$ lattice [42–44]. The substitution of Ni with Fe in $Ni(OH)_2$ induces the formation of NiFe hydroxide in LDH structure. After sulfidation, the characteristic diffraction peaks related to (003), (006), (012), (018), and (113) planes of α-$Ni(OH)_2$ disappears in the XRD pattern of FeNiS samples, while the (001), (102), (110) and (111) planes of β-$Ni(OH)_2$ still remain. It reveals that the S is highly like to incorporate into α-$Ni(OH)_2$ to replace the OH group. Consequently, the characteristic diffraction peaks of $FeNi_2S_4$ (JCPDS Card No. 47-1740) at 31.3°, 32.8°, 38.0°, 50.1°, and 54.9° show up in the FeNiS sample' XRD pattern. This result suggests that the successful formation of the FeNiS, and the S sulfidation is highly to take place at α-$Ni(OH)_2$ site.

The incorporation of S into [NiFe]-LDH is also confirmed by the XPS of FeNiS samples. First of all, the whole XPS spectrum shows the coexistence of Fe, Ni and S in FeNiS as compared with [NiFe]-LDH (Fig. S2). The binding energy peaks of Ni 2p3/2 and Fe 2p3/2 locate at 856.04 eV and 711.48 eV (Fig. 2(a) and (b)), respectively, indicating the presence of Ni^{+2} and Fe^{+3} in the FeNiS [25,38,40]. Based on the deconvoluted XPS peaks of the Ni and Fe elements in FeNiS, both the Ni and Fe peaks in FeNiS sample shift compared to

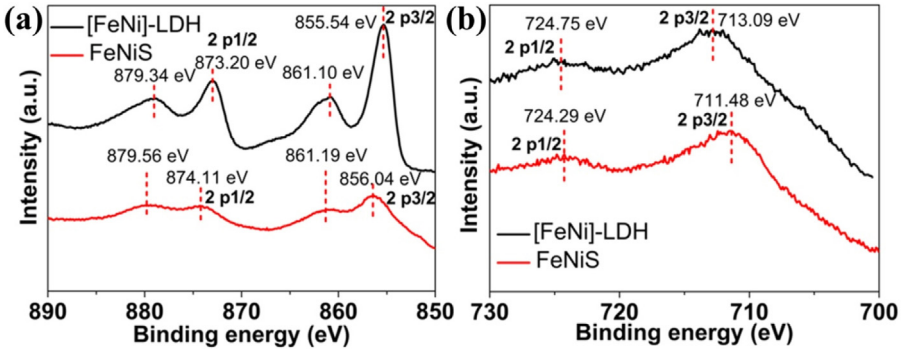

Fig. 2. XPS spectra of (a) Ni and (b) Fe region fitting of [NiFe]-LDH nanosheets and NiFeS nanopartilces.

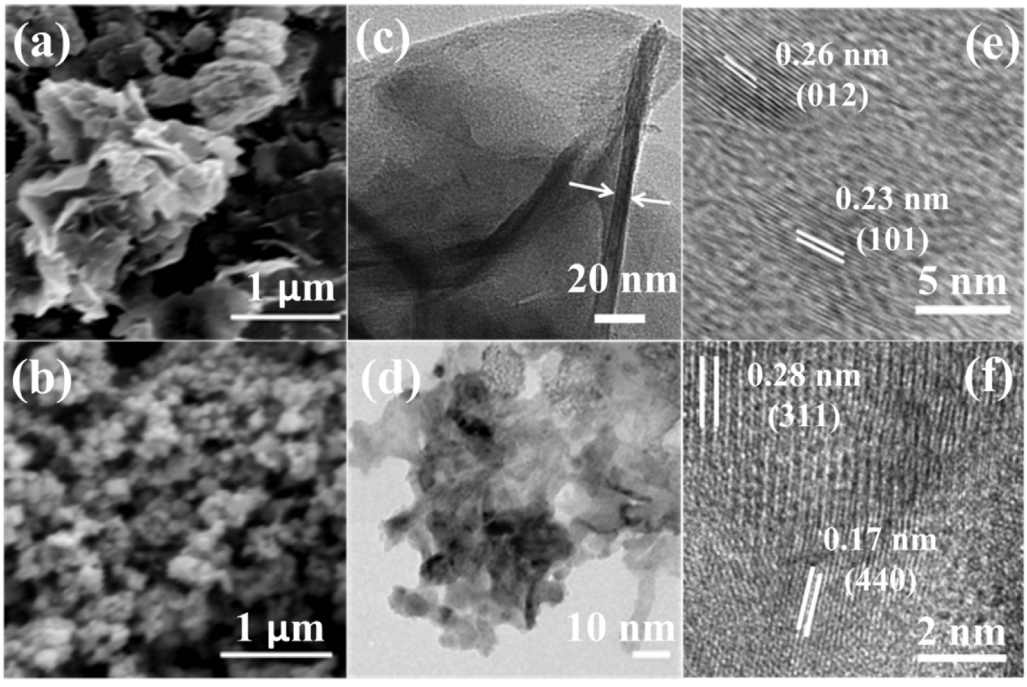

Fig. 3. Morphology and structure characterizations: SEM images, TEM images, and HRTEM images of [NiFe]-LDH nanosheets (a, c, e) and NiFeS (b, d, f) nanoparticles.

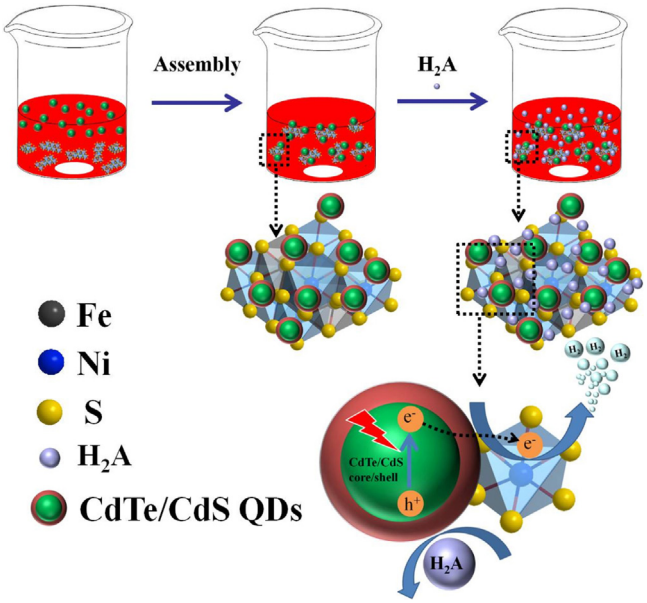

Fig. 4. The synthetic route to FeNiS-CdTe/CdS QDs system for the photocatalytic H_2 production.

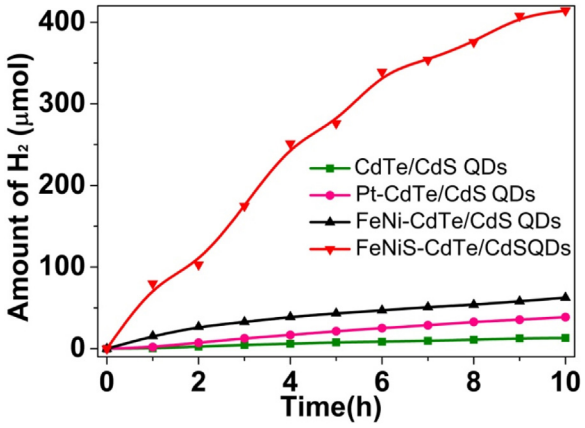

Fig. 5. H_2 evolution of CdTe/CdS QDs, Pt-CdTe/CdS QDs, FeNi-CdTe/CdS QDs and FeNiS-CdTe/CdS QDs under the optimized conditions.

[NiFe]-LDH, suggesting the change of chemical composition with S incorporation. Both the XRD and XPS results confirm the successful S incorporation in FeNiS samples.

With S incorporation, the morphology of NiFeS sample becomes significantly different from [NiFe]-LDH sample. SEM (Fig. 3a) and TEM (Fig. 3c) images show the nanosheets morphology of the [NiFe]-LDH with a mean lateral size of several hundred nanometers. From the standing LDH nanosheets, a thickness of [NiFe]-LDH is measured to be about 4 nm. In addition, HRTEM image of FeNi-LDH shows lattice fringes of (012) and (101) planes, which correspond to d = 0.26 and 0.0.23 nm, respectively. After the sulfuration treatment, SEM and TEM (Fig. 3b) shows these FeNiS samples become nanoparticles with rough surfaces in contrast to the smooth surfaces of the [NiFe]-LDH nanosheets. TEM images of FeNiS (Fig. 3d) presents the stacked nanoparticles with layered structure, which could be attributed to the breakage of nanosheets as previously reported [31,35,45]. HRTEM image (Fig. 1f) demonstrates that the lattice fringes with spacing of 0.28 and 0.17 nm indexed to (311) and (440) planes of FeNiS, corresponding to the transformation from α-phase $Ni(OH)_2$ and partial β-phase $Ni(OH)_2$ to FeNiS nanoparticles.

These FeNiS nanoparticles were utilized as an effective co-catalysts for photocatalytic H_2 evolution as shown in Fig. 4. This system is composed of FeNiS nanoparticles as a co-catalyst, CdTe/CdS QDs as a photosensitizer, and H_2A as the proton source and sacrificial electron donor. The FeNiS nanoparticles can contact well with CdTe/CdS QDs intimately to form the FeNiS-CdTe/CdS QDs composite with efficient charge transfer for H_2 evolution. H_2A is known to be able to provide electrons to regenerate CdTe/CdS QDs as well as protons for photocatalytic H_2 production in water. Obviously, the visible light-driven H_2 production is dependent on the solution pH, as well as the amount and ratio of H_2A and FeNiS nanoparticles. The optimized solution pH value for H_2 production is around pH = 4.5 as shown in Fig. S3 [46–48]. With pH = 4.5, the optimized H_2A concentration for H_2 evolution is ~20 mg/mL as shown Fig. S4. Without the FeNiS nanoparticles as co-catalysts, the H_2 production by CdTe/CdS QDs is very low as listed in Fig. S5. Once the CdTe/CdS QDs is anchored with FeNiS nanoparticles, the H_2 production is dramatically improved. It is reasonable because the deposition of FeNiS onto CdTe/CdS QDs would possess a plenty of active sites to promote the charge separation and lower the energy barrier for H_2 evolution. The ratios of FeNiS nanoparticels over CdTe/CdS also need optimize because the too few FeNiS cannot efficiently co-catalysis the H_2 evolution while overdosed FeNiS could block the light [49]. After optimization, photocatalytic H_2 evolution experiment is carried out under optimal conditions of CdTe/CdS QDs (CdTe, 6.5×10^{-6} M), FeNiS (0.15 mg/mL), and H_2A (20 mg/mL) at 20 ml buffer solution with pH = 4.5.

Fig. 5 shows the H_2 evolution with the exposure time of the photocatalysts under the optimized conditions. The FeNiS-CdTe/CdS QDs photocatalysts shows ~11 and ~6 times higher average H_2 evolution rate (41.4 μmol/h) than Pt-CdTe/CdS QDs (3.8 μmol/h) and FeNi-CdTe/CdS QDs (6.3 μmol/h), respectively. The low activities of Pt as co-catalyts for CdTe/CdS QDs could be ascribed to the sulfur surfactant on the surface of CdTe/CdS QDs. Although [FeNi]-LDH nanosheets are also highly active for electrochemical H_2 evolution, [FeNi]-LDH nanosheets do not effectively catalyze the H_2 evolution for CdTe/CdS QDs. The lower activities of [FeNi]-LDH nanosheets compared to FeNiS can be ascribed to two possible factors. First, the FeNiS is more effective for hydrogen evolution as demonstrated in previous report in electrolysis [25]. Second, the possible bad contact between the CdTe/CdS QDs and [FeNi]-LDH nanosheets for electron transfer. The good contact between the FeNiS and CdTe/CdS QDs can be obviously attributed to the more bonding sites and active sites of NiFeS to combine with CdTe/CdS QDs.

To further testify the above speculation and gain further information on the structure and composition of FeNi-CdTe/CdS and FeNiS-CdTe/CdS composites, XPS spectra of S and Cd are shown in Fig. 6a and b. S2p spectrum of CdTe/CdS can be well fitted with a single doublet with S2p1/2 peaking at 163.21 eV and S2p3/2 at 161.87 eV, respectively. After deposited the FeNiS, the S2p3/2 doublet further shift to 163.02 eV for S2p1/2 and 161.53 eV, respectively, which are attributed to the coordination of Fe/Ni with S group on the surface of CdTe/CdS QDs [50,51]. Meanwhile, the similar shifts were observed on FeNi-CdTe/CdS QDs. The S2p spectrum of FeNiS is consisted of S2p3/2 at 162.46 eV and S2p1/2 at 161.16 eV, which is coincident with divalent sulfide ions (S^{2-}). Higher binding energy of sulfur species at 169.14 eV is due to the oxidation of the sulfur species retained on the surface after the sulfidation, indicating a sulfur-associated surface reconstruction [45]. Therefore, the formation of sulfur species in FeNiS could also improve the sulfur tolerance. According to Fig. 5, FeNiS-CdTe/CdS exhibits much higher photocatalytic performance than Pt-CdTe/CdS (3.8 μmol/h) because Pt could be easily poisoned by S^{2-} on the surface of CdTe/CdS QDs. This result suggests that the FeNiS exhibits high sulfur tolerance as a great advantage over Pt as co-catalysts for CdTe/CdS QDs. Besides, the binding energy of S2p in FeNiS-CdTe/CdS shifts to 163.02 eV and 161.53 eV for S2p1/2 and

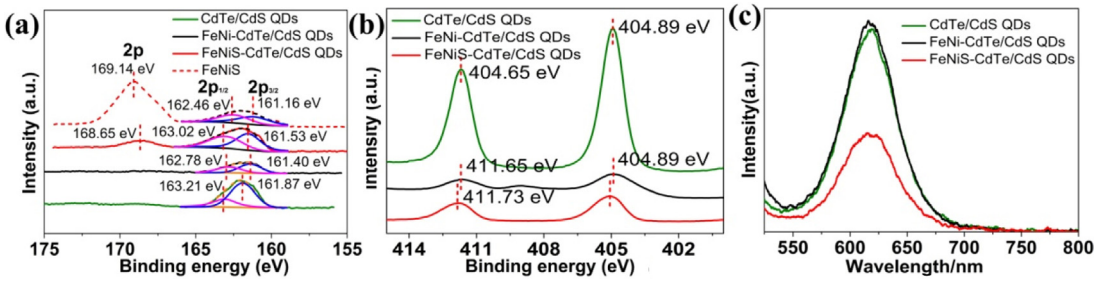

Fig. 6. High-resolution XPS spectra and fitted peaks of samples: Sulfur 2p (a) and Cadmium 3d (b) of CdTe/CdS QDs, FeNi-CdTe/CdS QDs and FeNiS-CdTe/CdS QDs. Emission spectra of CdTe/CdS QDs, FeNi-CdTe/CdS QDs and FeNiS-CdTe/CdS QDs containing CdTe/CdS QDs (CdTe, 6.5×10^{-6} M), pH 4.5, H_2A (20 mg/mL) and FeNiS (0.15 mg/mL) (c).

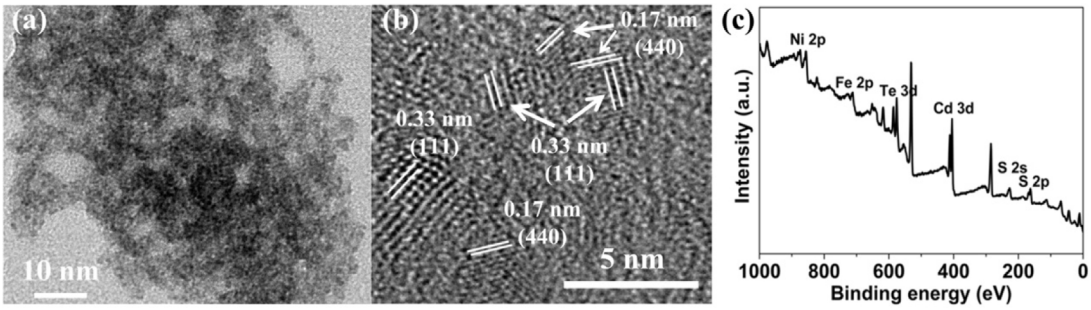

Fig. 7. TEM images (a) and HRTEM images (b) of FeNiS-CdTe/CdS QDs and XPS survey for FeNiS-CdTe/CdS QDs (c).

S2p3/2 (see Fig. 6a), respectively. The fitting results confirm the successful interaction of sulfur species from FeNiS and Cd^{2+} on the surface of CdTe/CdS QDs. The result is further confirmed by examining the Cd 3d spectra in Fig. 6b. The binding energy of Cd 3d in FeNiS-CdTe/CdS shifts 0.08 eV and 0.19 eV to higher binding energies for Cd 3d1/2 and Cd 3d5/2 compared to the CdTe/CdS, while for FeNi-CdTe/CdS, there is no obvious change of peaks belonging to Cd 3d1/2 and Cd 3d5/2 [52]. The effective junction of sulfur species and Cd^{2+} could promote the photogenerated charge separation and electron transfer more effective than [FeNi]-LDH. Since larger surface areas could provide more opportunities for the loading of CdTe/CdS QDs, it is important to figure out the impact of [FeNi]-LDH and FeNiS NPs' surface areas on H_2 evolution. As shown in Table S1, the surface area of [FeNi]-LDH is 55.06 m^2/g, which is larger than FeNiS NPs' BET area of 16.29 m^2/g. However, FeNiS-CdTe/CdS exhibits much higher photocatalytic performance than FeNi-CdTe/CdS QDs, which further conform that FeNiS provides more bonding sites and active sites for co-catalyze the CdTe/CdS QDs for hydrogen evolution. In an effort to further clarify the process, fluorescence of CdTe/CdS QDs, FeNi-CdTe/CdS QDs and FeNiS-CdTe/CdS QDs was carried out at the optimized condition with pH 4.5 (Fig. 6c). The PL of FeNiS-CdTe/CdS QDs is dramatically quenched as compared with FeNi-CdTe/CdS QDs, which is attributed to the efficient electron transfer from CdTe/CdS QDs to FeNiS. According to previous spectroscopic and electrochemical studies, the conduction band energy level (E_{cb}) of the CdTe QDs (3.5 nm determined by HRTEM) (−1.6 V vs NHE) is more negative than the redox potential of the Ni^{2+}/Ni^0 couples (−0.25 V vs NHE), Fe^{3+}/Fe^{2+} and Fe^{2+}/Fe^0 couples (−0.77 V and −0.44 V vs NHE), the free energy change of the electron transfer from the excited CdTe QDs to the active sites of Ni/Fe is thermodynamically favorable. [51,53,54]

In order to visualize the junction structure, FeNiS-CdTe/CdS composite was investigated by TEM and HRTEM. Compared with the structure of FeNiS nanoparticles in Fig. 3d, large amount of CdTe/CdS QDs with particle size of ~3 nm are evenly distributed on FeNiS nanoparticles (Fig. 7a). The magnified HRTEM image in Fig. 7b exhibits fringes with lattice spacing of 0.33 nm and 0.17 nm, which correspond to the (111) plane of CdTe/CdS QDs and the (440) plane of FeNiS, respectively. [27] Meanwhile, the elements analysis of Fe, Ni, S, Cd, and Te are confirmed in FeNiS-CdTe/CdS sample by XPS and ICP analysis (Fig. 7c and Table S2), which confirm the successful formation of FeNiS-CdTe/CdS QDs composite. The intimate contact between FeNiS and CdTe/CdS QDs is believed to improve the charge separation and therefore the photocatalytic activity. The above results further confirm that the combination of FeNiS nanoparticles and CdTe/CdS core/shell QDs is a promising strategy for preparing highly efficient photocatalysts for H_2 generation. To evaluate the durability of the FeNiS NPs, the photocatalytic H_2 evolution activity of FeNiS-CdTe/CdS was measured for 30 h. More than 576.9 μmol of H_2 (4437.5 TON for CdTe/CdS QDs) were generated over 30 h under visible light irradiation (Fig. S6), demonstrating the good stability of the FeNiS-CdTe/CdS. And the crystal phase of FeNiS remains unchanged according to the XRD analysis (Fig. S7). But, the H_2 evolution rate reduced slightly, which could be attributed to the photocorrosion of CdTe/CdS QDs.

4. Conclusions

In summary, the sulfurated [NiFe]-LDH (FeNiS) nanoparticles can be successfully constructed via a facile sulfur treatment of 2D [FeNi] LDH nanosheets and the FeNiS nanoparticles could be a better co-catalysts for CdTe/CdS QDs because they can provide more bonding sites for CdTe/CdS QDs than [FeNi] LDH nanosheets. The sulfur species as the bonding sites formed during the sulfidation process would not only improve the sulfur tolerance but also be connected with Cd^{2+} on the surface of CdTe/CdS QDs. The well contact of FeNiS and CdTe/CdS QDs would efficiently accelerate electrons transfer between CdTe/CdS QDs and FeNiS. The photocatalyst of FeNiS-CdTe/CdS QDs exhibits good photocatalytic activity and its intial H_2 evolution rate is up to 26.5 $\mu mol \cdot h^{-1} \cdot mg^{-1}$, which is much better than those using Pt or [FeNi] LDH as co-catalysts. In all, the FeNiS nanoparticles are a promising low cost co-catalyst for photocatalysis because of their large amount of bonding sites, active sites and high sulfur tolerance.

Acknowledgements

This worked is National Natural Science Foundation of China (Grant 51372151, 21303103, 21507083) and the Foundation of Shanghai Government (15PJ1404000).

Appendix A. Supplementary data

Supplementary data associated with this article can be found, in the online version, at http://dx.doi.org/10.1016/j.apcatb.2017.02.075.

References

[1] N. Armaroli, V. Balzani, Angew. Chem. Int. Ed. 46 (2007) 52–66.
[2] J. Barber, Chem. Soc. Rev. 38 (2009) 185–196.
[3] P. Du, R. Eisenberg, Energy Environ. Sci. 5 (2012) 6012–6021.
[4] S.J.A. Moniz, S.A. Shevlin, D.J. Martin, Z.-X. Guo, J. Tang, Energy Environ. Sci. 8 (2015) 731–759.
[5] D.G. Nocera, Energy Environ. Sci. 3 (2010) 993–995.
[6] W. Lubitz, W. Tumas, Chem. Rev. 107 (2007) 3900–3903.
[7] Y. Choquette, L. Brossard, A. Lasia, H. Menard, Electrochim. Acta 35 (1990) 1251–1256.
[8] M. Contestabile, G.J. Offer, R. Slade, F. Jaeger, M. Thoennes, Energy Environ. Sci. 4 (2011) 3754–3772.
[9] D. Gust, T.A. Moore, A.L. Moore, Acc. Chem. Res. 42 (2009) 1890–1898.
[10] N.S. Lewis, Science 315 (2007) 798–801.
[11] P.V. Kamat, J. Phys. Chem. C 112 (2008) 18737–18753.
[12] P. Zrazhevskiy, M. Sena, X. Gao, Chem. Soc. Rev. 39 (2010) 4326–4354.
[13] P.V. Kamat, K. Tvrdy, D.R. Baker, J.G. Radich, Chem. Rev. 110 (2010) 6664–6688.
[14] W.J. Youngblood, S.H.A. Lee, K. Maeda, T.E. Mallouk, Acc. Chem. Res. 42 (2009) 1966–1973.
[15] Z. Han, F. Qiu, R. Eisenberg, P.L. Holland, T.D. Krauss, Science 338 (2012) 1321–1324.
[16] J.X. Jian, Q. Liu, Z.J. Li, F. Wang, X.B. Li, C.B. Li, B. Liu, Q.Y. Meng, B. Chen, K. Feng, C.H. Tung, L.Z. Wu, Nat. Commun. 4 (2013) 2695.
[17] A. Das, Z. Han, W.W. Brennessel, P.L. Holland, R. Eisenberg, ACS Catal. 5 (2015) 1397–1406.
[18] F. Andolfatto, R. Durand, A. Michas, P. Millet, P. Stevens, Int. J. Hydrogen Energy 19 (1994) 421–427.
[19] A. Cornell, D. Simonsson, J. Electrochem. Soc. 140 (1993) 3123–3129.
[20] D. Galizzioli, F. Tantardini, S. Trasatti, J. Appl. Electrochem. 5 (1975) 203–214.
[21] J. Cheng, H. Zhang, H. Ma, H. Zhong, Y. Zou, Electrochim. Acta 55 (2010) 1855–1861.
[22] C. Wang, K.E. de Krafft, W. Lin, J. Am. Chem. Soc 134 (2012) 7211–7214.
[23] J.I. Goldsmith, W.R. Hudson, M.S. Lowry, T.H. Anderson, S. Bernhard, J. Am. Chem. Soc. 127 (2005) 7502–7510.
[24] N.P. Dasgupta, C. Liu, S. Andrews, F.B. Prinz, P. Yang, J. Am. Chem. Soc. 135 (2013) 12932–12935.
[25] X. Long, G. Li, Z. Wang, H. Zhu, T. Zhang, S. Xiao, W. Guo, S. Yang, J. Am. Chem. Soc. 137 (2015) 11900–11903.
[26] G. Abellán, C. Martí-Gastaldo, A. Ribera, E. Coronado, Acc. Chem. Res. 48 (2015) 1601–1611.
[27] D. Yue, X. Qian, Z. Zhang, M. Kan, M. Ren, Y. Zhao, ACS Sustain. Chem. Eng. 4 (2016) 6653–6658.
[28] D. Voiry, H. Yamaguchi, J. Li, R. Silva, D.C.B. Alves, T. Fujita, M. Chen, T. Asefa, V.B. Shenoy, G. Eda, M. Chhowalla, Nat. Mater. 12 (2013) 850–855.
[29] M.A. Lukowski, A.S. Daniel, C.R. English, F. Meng, A. Forticaux, R.J. Hamers, S. Jin, Energy Environ. Sci. 7 (2014) 2608–2613.
[30] Q. Wang, D. O'Hare, Chem. Rev. 112 (2012) 4124–4155.
[31] J. Jiang, S. Lu, H. Gao, X. Zhang, H. Yu, Nano Energy 27 (2016) 526–534.
[32] B.M. Hunter, W. Hieringer, J.R. Winkler, H.B. Gray, A.M. Muller, Energy Environ. Sci. 9 (2016) 1734–1743.
[33] H. Yin, Z. Tang, Chem. Soc. Rev. 45 (2016) 4873–4891.
[34] Y. Hou, M.R. Lohe, J. Zhang, S. Liu, X. Zhuang, X. Feng, Energy Environ. Sci. 9 (2016) 478–483.
[35] X. Jia, Y. Zhao, G. Chen, L. Shang, R. Shi, X. Kang, G.I.N. Waterhouse, L. Wu, C. Tung, T. Zhang, Adv. Energy Mater. 6 (2016), n/a–n/a.
[36] W. Zhou, L. Guo, Chem. Soc. Rev. 44 (2015) 6697–6707.
[37] J. Xiao, L. Wan, S. Yang, F. Xiao, S. Wang, Nano Lett. 14 (2014) 831–838.
[38] Z. Lu, W. Xu, W. Zhu, Q. Yang, X. Lei, J. Liu, Y. Li, X. Sun, X. Duan, Chem. Commun. 50 (2014) 6479–6482.
[39] X. Long, J. Li, S. Xiao, K. Yan, Z. Wang, H. Chen, S. Yang, Angew.Chem 126 (2014) 7714–7718.
[40] M. Gong, Y. Li, H. Wang, Y. Liang, J.Z. Wu, J. Zhou, J. Wang, T. Regier, F. Wei, H. Dai, J. Am. Chem. Soc. 135 (2013) 8452–8455.
[41] X. Long, S. Xiao, Z. Wang, X. Zheng, S. Yang, Chem. Commun. 51 (2015) 1120–1123.
[42] P. Axmann, O. Glemser, J. Alloys Compd. 246 (1997) 232–241.
[43] A.I. Khan, D. O'Hare, J. Mater. Chem. 12 (2002) 3191–3198.
[44] M. Taibi, S. Ammar, F. Schoenstein, N. Jouini, F. Fiévet, T. Chauveau, J.M. Greneche, J. Phys. Chem. Solids 69 (2008) 1052–1055.
[45] X. Chen, X. Wang, J. Xiu, C.T. Williams, C. Liang, J. Phys. Chem. C 116 (2012) 24968–24976.
[46] Z.J. Li, J.J. Wang, X.B. Li, X.B. Fan, Q.Y. Meng, K. Feng, B. Chen, C.H. Tung, L.Z. Wu, Adv. Mater. 25 (2013) 6613–6618.
[47] J. Bhattacharyya, S. Das, S. Mukhopadhyay, Dalton Trans. (2007) 1214–1220.
[48] Z.J. Li, X.B. Li, J.J. Wang, S. Yu, C.B. Li, C.H. Tung, L.Z. Wu, Energy Environ. Sci. 6 (2013) 465–469.
[49] D. Yue, T. Zhang, M. Kan, X. Qian, Y. Zhao, Appl. Catal. B-Environ. 183 (2016) 1–7.
[50] C. Li, Z. Li, S. Yu, G. Wang, F. Wang, Q. Meng, B. Chen, K. Feng, C. Tung, L. Wu, Energy Environ. Sci. 6 (2013) 2597–2602.
[51] Z. Li, X. Fan, X. Li, J. Li, C. Ye, J. Wang, S. Yu, C. Li, Y. Gao, Q. Meng, C. Tung, L. Wu, J. Am. Chem. Soc. 136 (2014) 8261–8268.
[52] Z. Li, J. Wang, X.-B. Li, X. Fan, Q. Meng, K. Feng, B. Chen, C. Tung, L. Wu, Adv. Mater. 25 (2013) 6613–6618.
[53] Q. Sun, Z. Ren, R. Wang, N. Wang, X. Cao, J. Mater. Chem. 21 (2011) 1925–1930.
[54] H. Zhao, L. Qian, X. Guan, D. Wu, G. Zhao, Environ. Sci. Technol. 50 (2016) 5225–5233.